JGR Oceans

RESEARCH ARTICLE
10.1029/2023JC020167

Key Points:

- The 2019 northeastern Pacific marine heatwave had various offshore physical, biogeochemical, and biological impacts
- Long-term multidisciplinary observing systems are necessary to provide a holistic view of extreme events

Supporting Information:

Supporting Information may be found in the online version of this article.

Correspondence to:

C. Kohlman,
kohlman@uw.edu

Citation:

Kohlman, C., Cronin, M. F., Dziak, R., Mellinger, D. K., Sutton, A., Galbraith, M., et al. (2024). The 2019 marine heatwave at Ocean Station Papa: A multi-disciplinary assessment of ocean conditions and impacts on marine ecosystems. *Journal of Geophysical Research: Oceans*, *129*, e2023JC020167. https://doi.org/10.1029/2023JC020167

Received 22 JUN 2023
Accepted 16 APR 2024

Author Contributions:

Conceptualization: Catherine Kohlman, Meghan F. Cronin, Adrienne Sutton
Data curation: Catherine Kohlman, David K. Mellinger, Adrienne Sutton, Moira Galbraith, Marie Robert, Jim Thomson, Zhang Dongxiao
Formal analysis: Catherine Kohlman
Funding acquisition: Catherine Kohlman, Meghan F. Cronin
Investigation: Catherine Kohlman, Meghan F. Cronin
Methodology: Catherine Kohlman, Meghan F. Cronin, Robert Dziak, David K. Mellinger, Adrienne Sutton
Project administration: Meghan F. Cronin
Resources: Meghan F. Cronin, Robert Dziak, Adrienne Sutton, Moira Galbraith, Jim Thomson, Zhang Dongxiao, LuAnne Thompson
Software: Robert Dziak, David K. Mellinger
Supervision: Meghan F. Cronin, Robert Dziak, Zhang Dongxiao, LuAnne Thompson

The 2019 Marine Heatwave at Ocean Station Papa: A Multi-Disciplinary Assessment of Ocean Conditions and Impacts on Marine Ecosystems

Catherine Kohlman[1], Meghan F. Cronin[2], Robert Dziak[3], David K. Mellinger[3,4], Adrienne Sutton[2], Moira Galbraith[5], Marie Robert[5], Jim Thomson[6], Zhang Dongxiao[2,7], and LuAnne Thompson[1]

[1]University of Washington, School of Oceanography, Seattle, WA, USA, [2]National Oceanic and Atmospheric Administration, Pacific Marine Environmental Laboratory, Seattle, WA, USA, [3]National Oceanic and Atmospheric Administration, Pacific Marine Environmental Laboratory, Newport, OR, USA, [4]Oregon State University, Cooperative Institute for Marine Ecosystems and Resources Studies and Marine Mammal Institute, Newport, OR, USA, [5]Fisheries and Oceans Canada, Institute of Ocean Sciences, Sidney, BC, Canada, [6]University of Washington, Applied Physics Laboratory, Seattle, WA, USA, [7]University of Washington, Cooperative Institute for Climate, Ocean, and Ecosystem Studies, Seattle, WA, USA

Abstract In the past decade, two large marine heatwaves (MHWs) formed in the northeast Pacific near Ocean Station Papa (OSP), one of the oldest oceanic time series stations. Physical, biogeochemical, and biological parameters observed at OSP from 2013 to 2020 are used to assess ocean response and potential impacts on marine life from the 2019 northeast Pacific MHW. The 2019 MHW reached peak surface and subsurface temperature anomalies in the summertime and had both coastal, impacting fisheries, and offshore consequences that could potentially affect multiple trophic levels in the Gulf of Alaska. In the Gulf of Alaska, the 2019 MHW was preceded by calm and stratified upper ocean conditions, which preconditioned the enhanced surface warming in late spring and early summer. The MHW coincided with lower dissolved inorganic carbon and higher pH of surface waters relative to the 2013–2020 period. A spike in the summertime chlorophyll followed by a decrease in surface macronutrients suggests increased productivity in the well-lit stratified upper ocean during summer 2019. More blue whale calls were recorded at OSP in 2019 compared to the prior year. This study shows how the utility of long-term, continuous oceanographic data sets and analysis with an interdisciplinary lens is necessary to understand the potential impact of MHWs on marine ecosystems.

Plain Language Summary Marine heatwaves (MHWs) are warmer than normal surface ocean temperature events. In 2019, a MHW occurred in the northeastern Pacific, and we utilized Ocean Station Papa (OSP), a multidisciplinary observing system in the Gulf of Alaska, to present the physical, biogeochemical, and biological impacts. Prior to reaching the MHW's warmest surface temperatures, the upper ocean exhibited a calm and stratified state, which facilitated the occurrence of exceptionally high sea surface temperatures. During the MHW, warm water was present well below the surface and extended throughout the water column. Prior to the MHW's warmest surface temperatures, we also observed indications of increased primary productivity through observed spikes in chlorophyll levels and reductions in nutrient concentrations. Due to data limitations, the connection between this heightened primary productivity and higher trophic levels remains unclear. Our study demonstrates the necessity of adopting holistic perspectives when seeking to understand the complexities of MHWs.

1. Introduction

Prolonged extreme sea surface temperature (SST) anomalies, or marine heatwaves (MHWs) (Hobday et al., 2016), are known to have a cascade of impacts on the ocean's physics, biogeochemistry, ecosystem, and marine life. MHWs are often examined using either models or satellite SST (Amaya et al., 2020; Bond et al., 2015; Capotondi et al., 2022; Holbrook et al., 2019), ocean color (Hayashida et al., 2020; Noh et al., 2022), gridded subsurface data (Scannell et al., 2020) or disparate observations (Bond et al., 2015). Here, we examine the 2019 MHW in the northeast (NE) Pacific using a long-term ocean time series from the Ocean Station Papa (OSP) observing node located near the epicenter of the NE Pacific MHWs. The meteorological, physical,

Validation: Moira Galbraith, Marie Robert, Jim Thomson
Visualization: Catherine Kohlman
Writing – original draft: Catherine Kohlman
Writing – review & editing: Catherine Kohlman, Meghan F. Cronin, Robert Dziak, Adrienne Sutton, Moira Galbraith, Marie Robert, Jim Thomson, Zhang Dongxiao, LuAnne Thompson

biogeochemical, and lower and higher trophic biological data enable us to consider the connections that can result in widespread biogeochemical and ecosystem impacts.

In the recent decade, two notable MHWs (Hobday et al., 2016) have been observed in the NE Pacific surrounding OSP. In the winter of 2013/2014, a MHW named the "Blob" was observed and persisted well into 2015 (Bond et al., 2015) with subsurface temperature and salinity anomalies lingering until 2018 (Scannell et al., 2020). The main drivers of the 2013–2015 MHW were weaker surface winds that resulted in reduced surface heat loss and limited horizontal and vertical mixing with colder water (Bond et al., 2015). Teleconnections from the Tropical Pacific likely forced these atmospheric anomalies (Bond et al., 2015; Capotondi et al., 2022; Di Lorenzo & Mantua, 2016; Hartmann, 2015; Holbrook et al., 2019, 2020). Based upon OSP biogeochemical observations from 2007 through 2018, Mogen et al. (2022) suggest that these 2013–2015 MHW drivers were also responsible for an observed decrease in surface oxygen (O_2) and dissolved inorganic carbon (DIC). The upper ocean changes associated with the 2013–2015 MHW had pronounced coastal and offshore impacts on marine biodiversity, ecosystems, and fishery economics (Bond et al., 2015; Cheung & Frölicher, 2020; Holbrook et al., 2019; Long et al., 2021; Smale et al., 2019).

After the SST anomalies of the 2013–2015 MHW dissipated, the NE Pacific experienced another MHW in 2019, referred to as the "Blob2.0" (Amaya et al., 2020). Similar to the 2013–2015 MHW, the 2019 MHW appeared to be driven in part by reduced surface-level winds resulting from large-scale atmospheric anomalies (Amaya et al., 2020). The 2019 MHW peaked in the summer and had larger SST anomalies than the 2013–2015 MHW owing to positive net surface heat fluxes and a record shallow mixed layer (Amaya et al., 2020). The entire water column was fresher and more stratified than in the 2013–2015 MHW, and the 2019 MHW was believed to be supercharged by reemerged subsurface temperature anomalies from the 2013–2015 MHW (Scannell et al., 2020).

Located at 50°N, 145°W, 1200 km offshore of Vancouver Island, B.C. Canada, OSP (Figure 1) is the site of one of the oldest multi-disciplinary time series (Harrison, 2002; Whitney et al., 1998; Whitney & Freeland, 1999) and is just north of the centers of the two aforementioned MHWs (Figures 2a and 2b). From 1949 through 1981 it was occupied by a weathership, and since 1956, the Canadian Department of Fisheries and Oceans (DFO) Line P Program has made ship-based oceanographic observations at OSP and along a transect from the coast to OSP. At present, Line P ship-based observations are taken three times a year—typically in February, June, and August (Freeland, 2007). The NOAA Pacific Marine Environmental Laboratory (PMEL) Ocean Climate Station (OCS) surface mooring time series began at OSP in June 2007. In 2010, a Waverider surface mooring was deployed at OSP by the University of Washington (UW) Applied Physics Laboratory (APL). In 2015, OSP was enhanced to become a global node of the National Science Foundation (NSF) Ocean Observatory Initiative (OOI), with the deployment of two flanking subsurface moorings and a subsurface profiling mooring. In 2015, NOAA deployed a Noise Reference Station (NRS) that records passive acoustics for monitoring whales and other marine mammals. Together, these time series allow for multi-disciplinary studies to understand the evolution and impacts surrounding extreme events, such as MHWs.

In this study, we use OSP as an open ocean natural laboratory to explore the ocean's physical, chemical, and biological responses to the 2019 MHW forcing. We present a holistic study of the 2019 MHW that analyzes the surface and subsurface temperature and stratification anomalies, including the recovery from the 2013–2015 MHW. We examine the potential relationships between the increased surface temperature, increased stratification, reduced ocean acidification, increased productivity, and possible linkages to higher trophic levels at OSP in the summer of 2019. This case study provides insight into the complex interconnections and potential impacts of extreme ocean warming events.

2. Materials and Methods

2.1. Identifying MHW Periods at OSP

We identified MHWs at OSP as events where the local 31-day low-passed boxcar filtered daily SST anomalies relative to the seasonal climatology exceed the 90th percentile, similar to the MHW definition in Hobday et al. (2016). Gaps less than 5-day were linearly interpolated prior to applying the 31-day filter. The climatology was calculated from the OSP NOAA surface mooring 31-day filtered SST time series from 2007 to 2020.

The following list describes the suite of in-situ (moored and shipboard) and satellite data along with methods for quantities that we used to assess the widespread multi-disciplinary effects of the 2019 MHW. A shortened

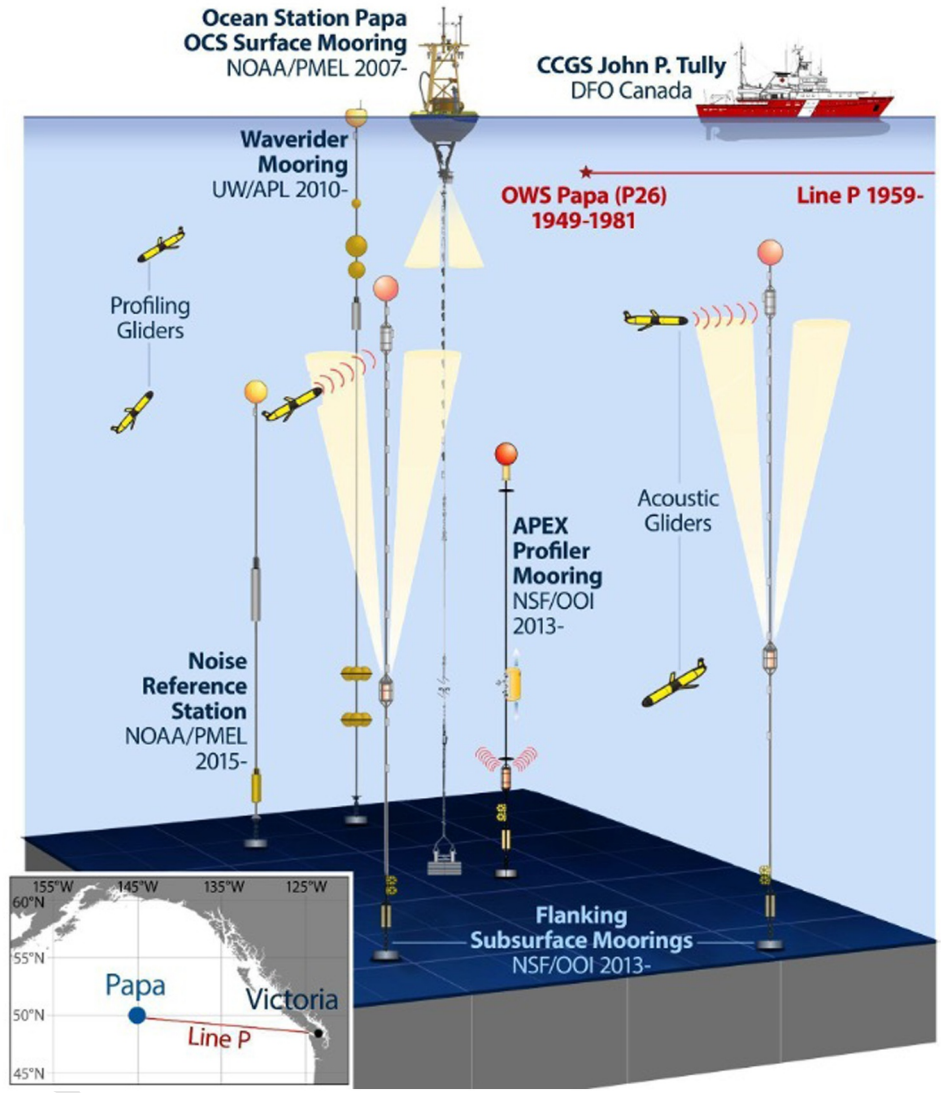

Figure 1. Illustration of the operational components of Ocean Station Papa and their respective names and locations. Reproduced with permission from Cronin et al. (2023). © 2023. This open access work is made available under the terms of the Creative Commons Attribution 4.0 International License (https://creativecommons.org/licenses/by/4.0/).

summary of the data is presented in Table 1. All climatologies are computed from a 31-day running average over the record length ending on 31 Dec 2020. Climatologies for subsurface salinity and temperatures were computed from nearby Argo floats profiles found within 49–51°N and 144–146°W between 1999 and 2022. All other climatologies are based upon the OSP time series. Anomalies on the 31-day running average time series in moored and gridded quantities are computed relative to these climatologies after filling gaps that are 5-day or less. Links to data sets used are found in the Data Availability section.

2.2. NOAA Surface Mooring

2.2.1. Surface Meteorological Variables, Temperature, Salinity, and Currents Data

Air-sea flux state variables (downwelling solar and longwave radiation, winds, surface currents, humidity, air and sea surface temperature, sea surface salinity, humidity, barometric pressure and rain); upper ocean temperature (at 23 depths from 1 to 300 m), salinity (at 21 depths from 1 to 300 m), computed potential density, and horizontal current time series at 35 m from the NOAA surface mooring at OSP are provided by the Ocean Climate Stations (OCS) Group (Cronin et al., 2015, 2023). Wind stress, evaporation, and latent and sensible heat fluxes are

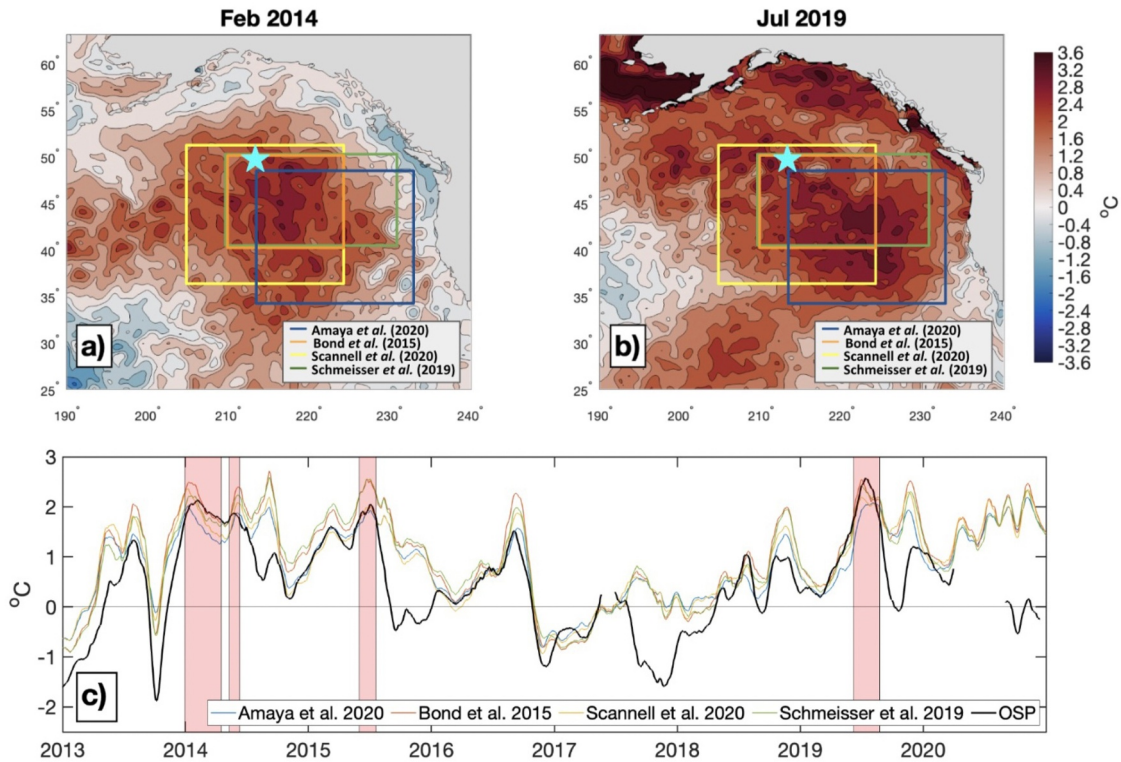

Figure 2. OISSTv2.1 daily sea surface temperature (SST) anomalies [°C] during (a) Feb 2014 and (b) Jul 2019. The blue star represents the location of OSP. (c) Observed SST anomalies from the NOAA surface mooring at OSP [°C; black solid line] overlaid upon area-averaged SST anomalies [°C] from OISSTv2.1 from areas defined in other studies (Amaya et al., 2020, pp. 34–47°N and 147–128°W; Bond et al., 2015, pp. 40–50°N and 150–130°W; Scannell et al., 2020, p. 35.5–51.5°N and 154.5–135.5°W and Schmeisser et al., 2019, pp. 40–50°N and 150–130°W) plotted in various colors (see legend). The red shading indicates 'MHW periods' (see methods). The tick marks on the horizontal axis are placed on Jan 1 of the year shown.

computed hourly using the Fairall et al. (2003) COARE 3.0b algorithm, and net surface heat flux is estimated as described in Cronin et al. (2015).

2.2.2. Seawater pCO_2 and Surface pH

Surface water pCO_2 (the partial pressure of CO_2 in air in equilibrium with the seawater at sea surface temperature) and surface seawater pH time series are from the Pacific Marine Environmental Lab (PMEL) Carbon Group (Sutton et al., 2012, 2014, 2016). Both variables were collected autonomously every 3-hr.

2.2.3. Bandpassing

To extract near-inertial currents from 35 m hourly currents observed at the OSP NOAA surface mooring, we utilized bandpass filtering to isolate near-inertial frequency components. The high-pass of the triangular filter was defined to be 7-hr (~0.5 times the inertial period), and the low-pass of the filter was set to 23 hr (~1.5 times the inertial period at 50°N).

2.2.4. Computing Dissolved Inorganic Carbon

To analyze the carbon system during the study period, the surface dissolved inorganic carbon (DIC) was computed from daily averaged surface water pCO_2, surface pH, sea surface salinity, and sea surface temperature from the NOAA surface mooring at OSP. The program used to compute the surface DIC was the MATLAB-version (v1.1) of CO2SYS (Lewis & Wallace, 1998; van Heuven et al., 2011) with the borate-to-salinity ratio of Dickson (1990), sulfate dissociation constants of Dickson (1990), and the carbonic acid dissociation constants of Dickson and Millero (1987) - refit data of Mehrbach et al. (1973).

Table 1
Summary of Data Sets, Variables, and Climatologies Used in Study

Data source	Variables used in study	Length of operation	Climatology
NOAA OSP Surface Mooring	Surface meteorological variables (winds, air temperature, humidity, barometric pressure, downwelling solar and longwave radiation, rain), bulk air-sea momentum, heat, and moisture fluxes, seawater temperature (surface to 300 m), salinity (surface to 300 m), surface and 35 m currents, surface air and seawater *p*CO2 and surface pH	2007 - Present	Sea surface temperature and meteorological variables: 2007 - 2020 Subsurface temperature and salinity: ARGO floats within 49–51°N and 144–146°W: 1999–2020 Currents, *p*CO2, and pH: N/A
NSF OOI Global Station Papa Array's Flanking Moorings A and B	Deep (300–1500 m) subsurface temperature and salinity observations	2013 - Present	ARGO floats within 49–51°N and 144–146°W: 1999 - 2020
APL-UW Waverider Mooring	Significant wave height	2010 - Present	2010–2020
DFO Line P shipboard data	*Euphausia pacifica* dry weight biomass, chlorophyll concentrations, nitrate plus nitrite, sulfite, and oxygen observations at Station P26	1959 - Present	PACIFICA nitrate and silicate: 1985 - 2008 *Euphausia pacifica* dry weight biomass and chlorophyll: N/A
OOI Various Cruises	Supplemental chlorophyll, oxygen, nitrate plus nitrite, and sulfite	2013 - Present	N/A
NOAA Noise Reference Station Mooring	Blue whale B call counts	2015 - Present	N/A
NOAA ¼ degree daily Optimum Interpolation Sea Surface Temperature (OISST) v2.1 data	Sea surface temperature	1981 - Present	1982–2010

Note. If no climatology was used, "N/A" is displayed.

2.2.5. Computing Mixed Layer

The mixed layer depths at OSP were computed using methods described in Cronin et al. (2015) using daily averaged temperature and salinity profiles from the OSP surface mooring. Mixed layer depth is defined as the depth where density is 0.03 kg m^{-3} denser than that found at 10 m depth. An isothermal layer depth, defined as the depth where temperature is 0.2°C cooler than found at 10 m depth, is also computed. A barrier layer exists when the mixed layer depth is salinity stratified and shallower than the isothermal layer (de Boyer Montégut, 2004; Katsura et al., 2015; Lukas & Lindstrom, 1991).

2.2.6. Computing Saturation Equilibrium Oxygen

The saturation equilibrium oxygen in seawater was computed using the Gibbs SeaWater (GSW) Oceanographic MATLAB Toolbox (McDougall & Barker, 2011) with inputs of absolute salinity (computed from density and in-situ temperature) and conservative temperature (computed from absolute salinity and in-situ temperature). The GSW Toolbox uses solubility coefficients from Benson and Krause (1984) as fitted by Garcia and Gordon (1992, 1993).

2.3. NSF OOI Subsurface Moorings

Deep (300–1500 m) subsurface temperature and salinity observations were provided by the NSF OOI Global Station Papa Array's Flanking Moorings A and B. These two flanking moorings are located within 60 km of the NOAA surface mooring and contain CTDs collecting data every 15 min at discrete depths from 30 m below the surface to 1500 m. Deep (300–1500 m) profiles (Figure 3a) were created by averaging the daily averaged values between the Flanking Subsurface Moorings A and B.

2.4. APL-UW Waverider Mooring

Daily significant wave height time series data from the Waverider mooring at OSP were provided by the APL-UW Waverider Group. The Waverider collects pitch roll and heave displacements at 1.28 Hz at 30-min intervals (Thomson et al., 2013). Spectral moments are computed onboard and then transmitted to the Coastal Data

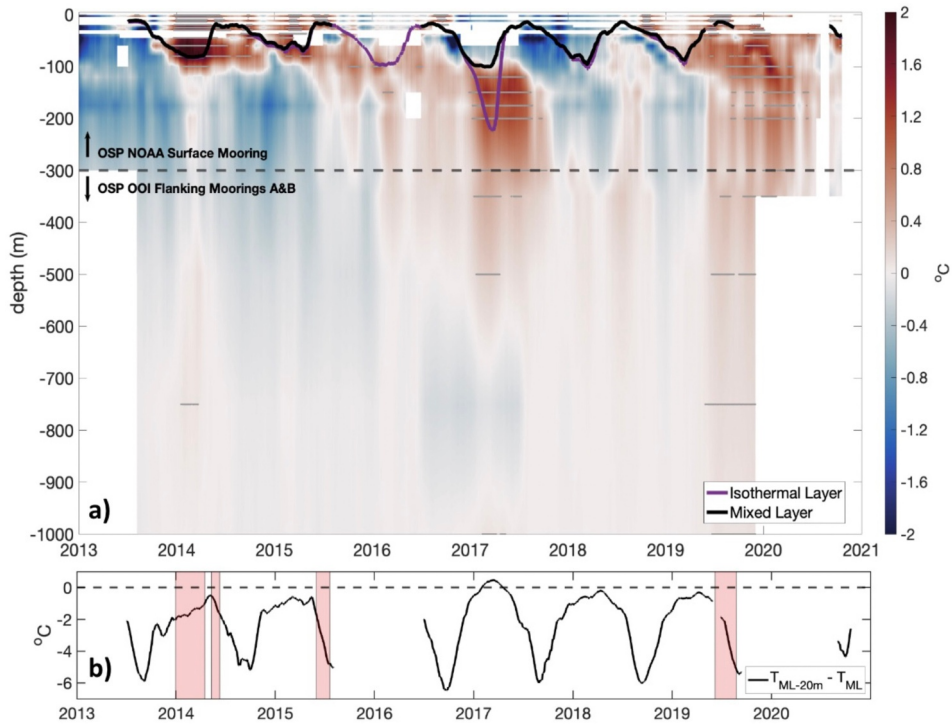

Figure 3. (a) Subsurface temperature anomalies [°C] at OSP. Data from the surface to 300 m are from the OSP NOAA surface mooring, and data below 300 m are averaged from OSP OOI Flanking Moorings A and B. Subsurface anomalies computed from 1999 to 2020 Argo climatology. Base of deep isothermal layer [m; purple solid line] and base of shallow isopycnal mixed layer depth (MLD) [m; black solid line] are overlaid. Subsurface temperature anomalies exceeding the 90th percentile of the seasonal climatology at a given depth are marked by gray line segments. (b) Temperature difference between the mixed layer and 20 m below the mixed layer [°C]. Data are shown as a 31-day running average.

Information Program (CDIP) at the Scripps Institution of Oceanography. These buoy data are publicly available as CDIP Station 166 and National Data Buoy Center (NDBC) Station 46,246.

2.5. Ship Data

2.5.1. DFO Line P Shipboard Data

Station P26, at OSP, is the farthest offshore station of the "Line P" survey line. This study includes *Euphausia pacifica* dry weight biomass (from *E. pacifica* abundance; Mackas, 1995), chlorophyll concentrations, nitrate plus nitrite (nitrite measurements are so small, <0.3 μM, that nitrate plus nitrite can be expressed as nitrate for simplicity; Whitney et al., 1998), silicate, and oxygen observations at Station P26 for insight into biological activity at OSP. Data displayed as 'surface' refers to the depth integrated values from the air-sea interface to 5 m depth. There are three Line P cruises per year generally in February, June, and August. The Line P data are managed and coordinated by the Institute of Ocean Sciences from Fisheries and Oceans Canada (DFO). Data submitted to PACIFICA from NCEI (Suzuki et al., 2013), within 49–51°N and 144–146°W, are used as a 1985–2008 climatology for nitrate plus nitrite, sulfite, and oxygen.

2.5.2. OOI Various Cruises

Supplemental chlorophyll, oxygen, nitrate plus nitrite, and sulfite cruise ship samples at OSP are included from OOI's shipboard data log ranging from July 2013 to present with about one cruise per year, generally in late summer.

2.6. NOAA Noise Reference Station Mooring: Autonomous Hydrophone Data and Whale Call Detection

The hydrophone recording package used to collect ambient acoustic data at the OSP Noise Reference Station (NRS) subsurface mooring consists of a single ceramic hydrophone with a filter/amplifier, clock, and a low-power processor, all powered by an internal battery pack. The hydrophone (model ITC-1032) is omnidirectional with a nominal sensitivity of −192 dB re 1 V μPa^{-1}. The instrument records at a sampling rate of 5 kHz with 16-bit resolution, providing a continuous record of ocean ambient sound levels from July 2018 to September 2020. The pre-amplifier has an eight-pole anti-aliasing filter at 2.5 kHz with a filter curve to equalize the spectrum against typical ocean noise over the passband (Dziak et al., 2019). A low power cesium atomic clock with an average time drift of ∼0.1 s $year^{-1}$ was used for internal timing. The NRS sensor was located at 900 m within the ocean sound channel, with the goal of maximizing the detection range of biological sound sources.

The seasonal, acoustic presence of blue whales in the northeastern Pacific has been established in previous studies using hydrophone recordings of their vocalizations (Stafford et al., 2009). To detect recent blue whale call presence using the moored hydrophone at OSP, we used spectrogram correlation techniques (Mellinger & Clark, 2000) to target the tonal parts of the blue whale B call at signal frequencies between 25 and 26.5 Hz and time durations between 2.5 and 15 s in duration. The B call is suggested to be a result of pneumatic air bursts from the whales opening and closing respiratory air valves and can be used to identify the presence of blue whales (Dziak et al., 2017). The whale detection analysis was run in Ishmael (V.2.3.1) (Mellinger, 2001) over the 2 years of continuous hydrophone data at OSP (2018–2020). To identify the B call, a two-dimensional synthetic kernel is constructed and cross-correlated with a spectrogram of a recording, producing a recognition function—the likelihood at each point in time that the sound type was present. A threshold is then applied to this function to obtain discrete detection events, which are discrete points in time when the B call was likely present. The same spectrogram correlation method was used to detect sperm whale clicks, with the kernel adjusted in frequency and time to capture the short duration (<0.5 s) broadband (∼100–500 Hz) signal character of the clicks (Mellinger, 2004).

2.7. Gridded SST Data

The NOAA ¼ degree daily Optimum Interpolation Sea Surface Temperature (OISST) v2.1 data (Huang et al., 2020) were used to display locations of SST anomalies associated with the 2013–2015 and 2019 MHWs as well as a time series of SST anomalies associated with other studies, computed from the 1982–2010 climatology. The OISSTv2.1 data available from 1 September 1981 until the present are a combination of observations from different satellites, ships, buoys, and Argo floats interpolated to produce a spatially complete global SST map.

3. Results

3.1. Surface and Subsurface Anomalies

The general spatial pattern of SST anomalies for the 2013–2015 MHW (Figure 2a) and the 2019 MHW (Figure 2b) are similar. The centers of each event are generally located south of Anchorage, AK USA and west of Oregon USA. Centered in the Gulf of Alaska, OSP provides in-situ observations that create a unique natural laboratory for understanding MHWs. Although OSP is generally along the northernmost boundary for many studies that have analyzed NE Pacific MHWs properties as area averaged over a region defined by a surface box (i.e., Amaya et al., 2020, Bond et al., 2015, Scannell et al., 2020; Schmeisser et al., 2019) hereafter referred to as 'area-averaged' studies (Figures 2a and 2b), the observed SST anomalies at the NOAA surface mooring at OSP align well with area-averaged studies using satellite data, identifying the periods of peak anomalies for each MHW (Figure 2c). The red shading in the time series in Figure 2c represents MHW periods (see methods) that were observed at the NOAA surface mooring (in black) and area averaged OISSTv2.1 SST anomalies defined by various other studies (colored) from 2013 to 2020. During the 2013–2015 MHW period, three MHW periods were observed at OSP, all part of the 2013–2015 MHW event. The longest period of high SST anomalies at OSP occurred from 30 Dec 2013, to 17 Apr 2014. The high anomalies persisted for 109 days and reached a maximum SST anomaly of 2.1°C. The 2019 MHW was observed at OSP from 8 Jun 2019, to 25 Aug 2019 (79 days) with a peak SST anomaly of 2.6°C.

Both 2013–2015 and 2019 MHWs had anomalous surface and subsurface temperature signatures at OSP. Scannell et al. (2020) suggest that the 2019 subsurface temperature anomalies may be a signature of subducted

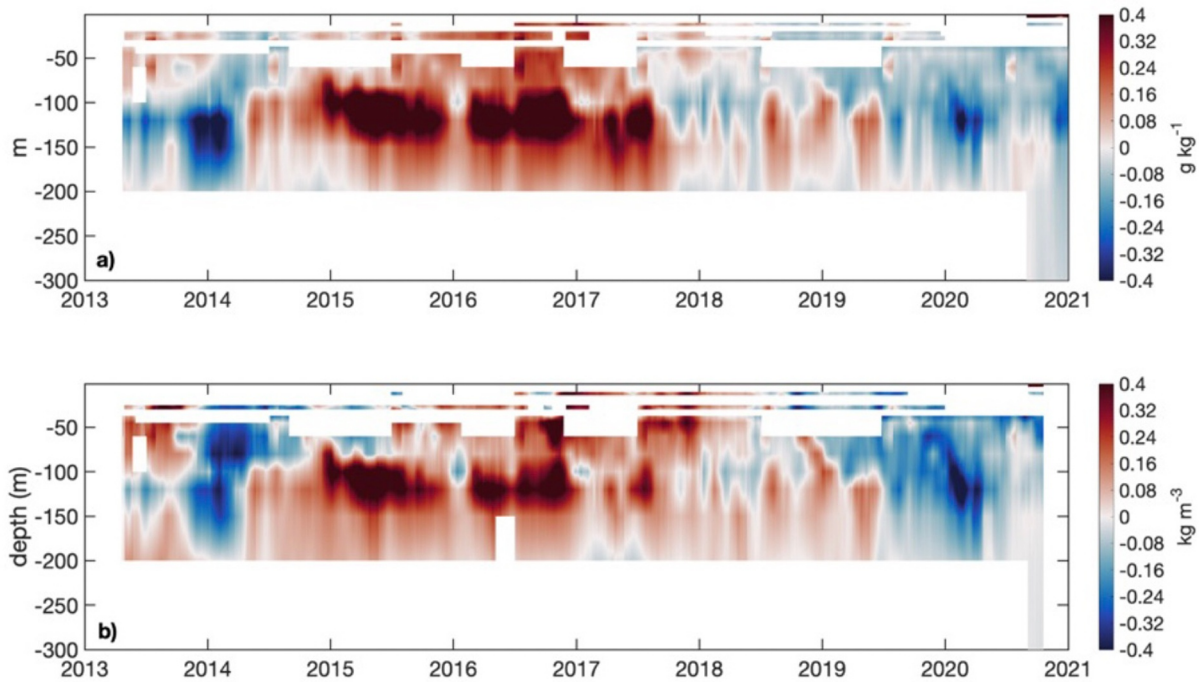

Figure 4. (a) Subsurface salinity anomalies [g kg^{-1}] and (b) potential density anomalies [kg m^{-3}] computed from subsurface temperature and salinity profiles observed from the NOAA surface mooring at OSP. Subsurface anomalies computed from 1999 to 2020 ARGO climatology. Data are shown as a 31-day running average.

warm surface anomalies from the 2013–2015 MHW. Subsurface temperature anomalies recorded at the NOAA surface mooring and OOI subsurface moorings at OSP during the start of the first MHW in late 2013 and early 2014 were strongest above the mixed layer depth (MLD) (i.e., the black line in Figure 3a above ∼100 m) and persisted until 2017. In the winter and spring of 2017, deeper waters (120–300 m) remained anomalously warm (gray line segments in Figure 3a). Further, this subsurface temperature anomaly persisted at least to 2018 and possibly regionally to 2019 as a result of being shielded from winter surface cooling by anomalously strong stratification and a fresher surface layer. As shown in Figure 3, during the winter of 2017 an extraordinarily thick "barrier layer", approximately 140 m thick, is found at OSP along with a temperature inversion present from Feb 2017 to Apr 2017 (Figure 3b). Here we define a barrier layer as when the MLD is salinity stratified and shallower than the isothermal layer (de Boyer Montégut, 2004; Katsura et al., 2015; Lukas & Lindstrom, 1991). Turbulent mixing and entrainment that eroded the MLD in this case caused the warm anomalies to re-emerge and "supercharge" the 2019 MHW. During the 2019 MHW, subsurface anomalously warm waters extended down to 1000 m, likely associated with a downward heaving of the thermocline associated with large-scale changes in the circulation. The vertical structure of the 2019 MHW varies in time at OSP. The warm anomalies were more confined to the surface ocean leading up to July 2019 before being present throughout the entire column (a "subsurface-reversed" followed by a "deep" MHW as defined in Zhang et al., 2023).

The upper ocean was anomalously stratified preceding the 2019 MHW (as early as mid-2018 to the summer of 2019), as seen by the anomalously less dense (blue) waters above the anomalously denser waters (red) in Figure 4b. Mid-2017 onward, there were fresher than normal conditions in the upper 100 m of the ocean at OSP overlying a warm subsurface temperature anomaly (Figure 4a). Scannell et al. (2020) suggest that these fresh anomalies were a result of increased freshwater input from precipitation in the Gulf of Alaska; however, there was not an increase in precipitation at OSP (Figure S1 in Supporting Information S1). Together, the surface ocean warm and fresh anomalies worked together to anomalously stratify the upper ocean in the winter of 2018/2019. The increase in stratification inhibited entrainment of deeper cooler waters, leading to favorable conditions for extreme SSTs.

Calm and stratified conditions preceding the summer of 2019 created favorable conditions for the 2019 MHW. Observed weaker wind stress magnitude and smaller significant wave height anomalies (Figures 5a and 5b)

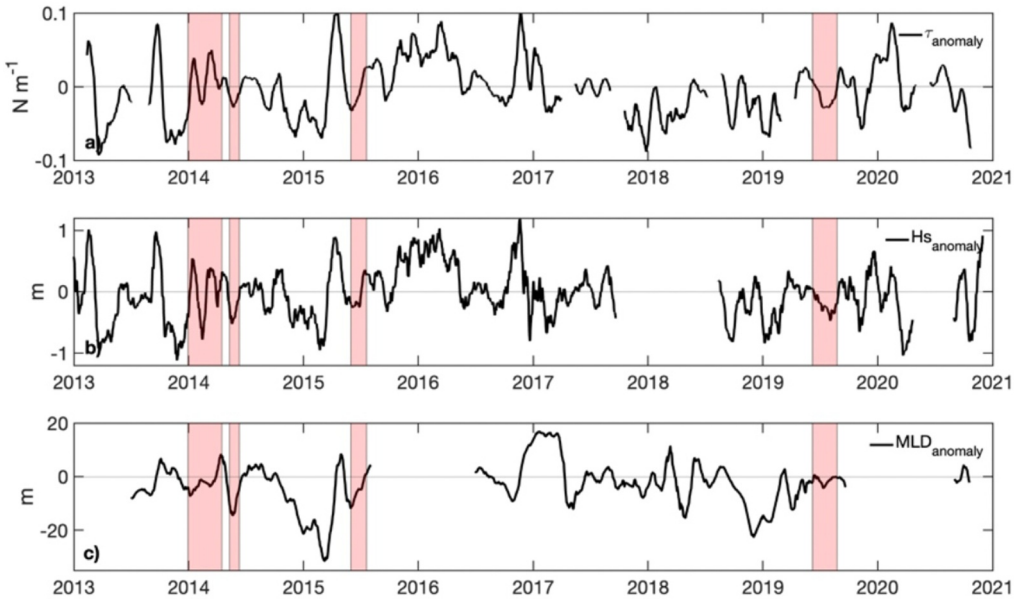

Figure 5. (a) Wind stress [N m^{-2}] observed from the NOAA surface mooring, (b) significant wave height [m] observed from the APL-UW Waverider mooring, and (c) mixed layer depth [m] anomalies observed from the NOAA surface mooring at OSP. A negative mixed layer depth anomaly represents a shallower mixed layer. Data are shown as a 31-day running average. The red shading represents observed MHW periods.

suggest calmer surface conditions that likely reduced wind-driven turbulence and mixing during the winter of 2018/2019 and summer of 2019. These significant wave height anomalies are also included here as an integral measure of the regional winds in that they include not only local wind generated waves, but also swell (Belka et al., 2014). The calmer conditions result in shallower winter and summer MLD (Figure 5c). Although the OSP 2019 summer MLD anomaly may appear small (5–6 m), the typical summer MLD (taken from the 2007–2020 climatology) at OSP reaches depths of about 10–13 m, suggesting roughly a 50% shoaling. The anomalously shallow winter mixed layer observed in 2018/2019 followed by reduction in wind-driven turbulence and shallow mixed layer in the summer of 2019 suggest a reduction of entrainment of cool, deeper waters into the upper ocean during the winter prior to the 2019 MHW, creating conditions favorable for warm upper ocean temperatures.

At OSP, the surface heat flux anomalies leading up to the 2019 MHW do not show as large a signal as anticipated (Figure 6) based on other air-sea flux analyses of the initiation of NE Pacific MHWs (Amaya et al., 2020; Schmeisser et al., 2019). These studies, which interpret the large anomalous net surface heat flux to be major drivers in the 2019 MHW were based on area-averaged studies with an emphasis on the region south of OSP (Figures 2a and 2b). At OSP, the net heat fluxes were anomalously positive (into the ocean) in May and June of 2019 prior to the MHW (Figures 6a and 6b), largely due to contributions from shortwave radiative fluxes (Figure 6c). During the 2019 MHW period, there was anomalous net heat flux out of the ocean, rather than into the ocean, as expected.

During the summer of 2019, there was a sudden weakening and shift from eastward to westward flow (Figure 7a). From early 2017 through the spring of 2019, the 35 m currents at OSP were generally eastward (positive zonal currents), in the direction of the North Pacific Current (Cummins & Freeland, 2007). This shift from eastward to westward flow in 2019 was not found during the 2013–2015 MHW. During the 2019 MHW, the changes in current direction may have reduced horizontal advection of cooler temperatures from west of OSP. Following this shift in zonal currents in mid-2019, the westward flow continued into the winter of 2019/2020. Although of lesser magnitude in summer 2019 compared to the 2013/2014 winter, there were also northward currents at OSP that might have advected warmer water into the region from the south (Figure 7a).

Higher energy near-inertial waves are typically observed at OSP during the winter season owing to the increased frequency of storms in winter (Alford et al., 2012). At OSP, the 35 m near-inertial currents are largest from October to January (Figure 7b). However, during the winter 2018/2019, there were slightly smaller near-inertial

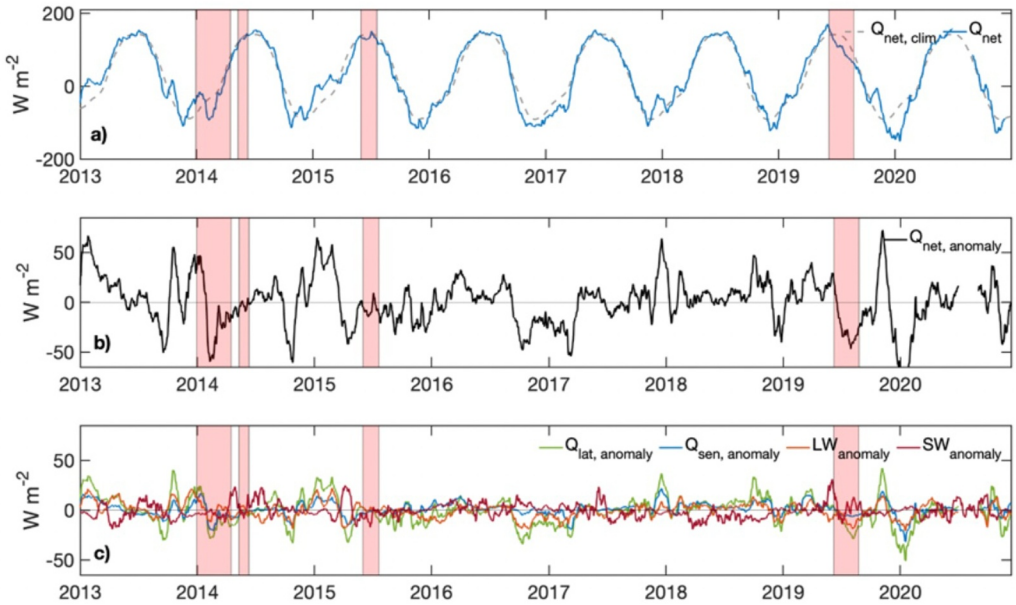

Figure 6. (a) Net heat flux [$Q_{net} = SW_{net} - Q_{lat} - Q_{sen} - LW_{net}$], (b) net heat flux anomalies, and (c) latent heat flux anomalies (green), sensible heat flux anomalies (blue), longwave radiative anomalies (orange), and shortwave radiative anomalies (red) from the NOAA Surface Mooring at OSP. A positive flux anomaly warms the ocean. Data are shown as a 31-day running average. The red shading represents MHW periods.

currents (as seen by smaller high frequency currents in 2018/2019 winter compared to 2016/2017 and 2017/2018 winters). This suggests that the weaker winds and inertial currents resulted in a more stably stratified water column. This may have contributed to persistence of the surface water temperature anomalies and the delayed subduction of the warmer subsurface temperatures (Figure 3a) as speculated by Scannell et al. (2020). The lower energetic near-inertial currents in 2018/2019 winter could have also resulted in weaker mixing and less entrainment of colder subsurface water. The resulting strong surface stratification could have contributed to the 2019 MHW.

3.2. Ecosystem Impacts

Similar to the conditions observed during 2013–2015 MHW (Mogen et al., 2022), we find low surface DIC and pCO_2 along with high surface pH during the 2019 MHW (Figure 8). The strong stratification and circulation changes could have contributed to the decrease in DIC similar to the 2013–2015 MHW (Mogen et al., 2022).

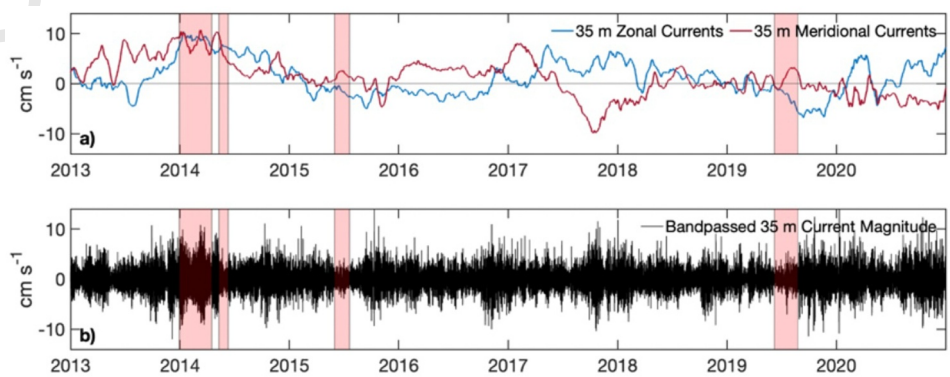

Figure 7. (a) Total zonal and meridional 35 m currents [cm s^{-1}] and (b) near-inertial 35 m current magnitudes [cm s^{-1}] observed from the NOAA surface mooring at OSP. The zonal and meridional current data are shown as a 31-day running average. The red shading represents observed MHW periods.

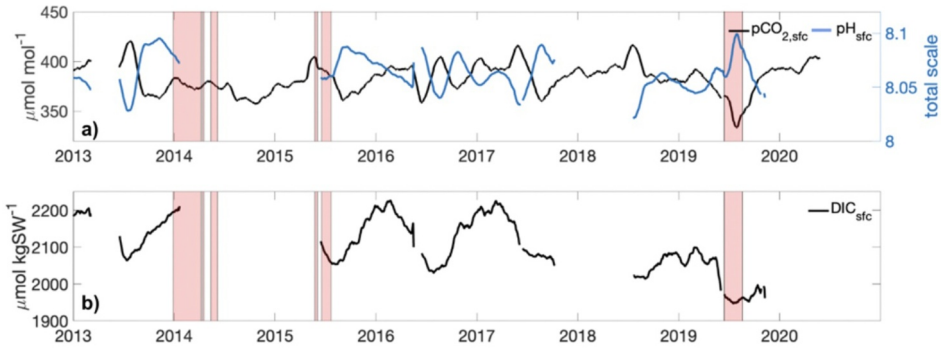

Figure 8. (a) Seawater pCO_2 [μmol mol^{-1}] and surface seawater pH [total scale] and (b) surface dissolved inorganic carbon (DIC) [μmol $kgSW^{-1}$] observed from the NOAA surface mooring at OSP. Data are shown as a 31-day running average. The red shading represents observed MHW periods.

Relatively large negative Apparent Oxygen Utilization (AOU) (oxygen concentration at saturation equilibrium minus observed oxygen) surface values were observed during the June cruise of 2019 (Figure 9a), suggesting that more oxygen was available in the water than what is expected based on the water's physical properties, which could be an indication of increased biological productivity.

An unusual increase of productivity was observed by cruise samples taken before and after the peak of the 2019 MHW. Surface chlorophyll and macronutrients (nitrate and silicate) from Line P cruises at P26 were used as indicators of productivity occurring at OSP (Figure 9). Notable large amounts of chlorophyll at OSP were observed in June 2016 (~1.19 mg m^{-3}), August 2017 (~1.28 mg m^{-3}), and June 2019 (~1.08 mg m^{-3}) as seen in Figure 9b. The large amount of chlorophyll in 2016 coincides with a negative AOU value in Figure 9a and was followed by a decrease in macronutrients (Figures 9c and 9d). The 2017 chlorophyll bloom occurred directly following the observed spring barrier layer (Figure 3a), and a decrease in nitrate and a depletion of silicate were observed directly following as well (Figure 9). The macronutrients again decreased in 2019 (with observed depletion of surface nitrate), coinciding with the observed June 2019 chlorophyll.

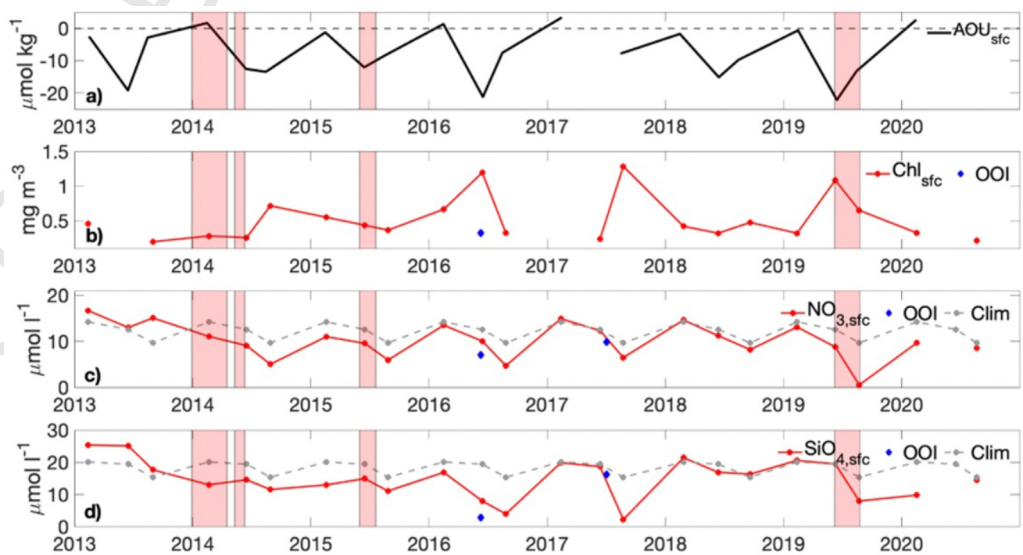

Figure 9. Surface (a) Apparent Oxygen Utilization (AOU) [μmol mol^{-1}] (computed oxygen concentration at saturation from the NOAA surface mooring at OSP minus observed oxygen from Line P Station P26 shipboard data), (b) chlorophyll [mg m^{-3}], (c) nitrate [μmol l^{-1}], and (d) silicate [μmol l^{-1}]. Line P Station P26 shipboard data are represented in red. OOI shipboard data are represented as blue diamonds. For nitrate and silicate, the PACIFICA 1985–2008 climatology is represented as gray dashed lines. The red shading represents observed MHW periods.

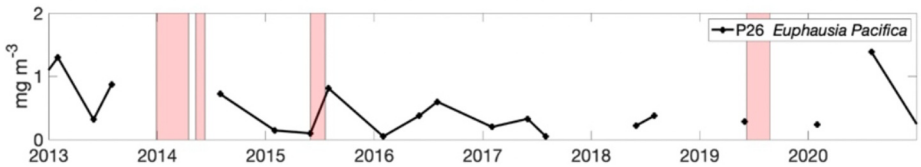

Figure 10. Shipboard *E. pacifica* biomass [mg m^{-3}] from Line P Station P26 250 m to surface bongo net. The red shading represents observed MHW periods.

Typical decreases in surface nitrate (6.9–7 μM) and silicate (11.1–11.5 μM) are indicators of primary productivity in the Gulf of Alaska (Harrison et al., 1999, 2004; Wong et al., 1998). Between the June and August cruises in 2019, there was a 12.6 μM decrease in nitrate (Figure 9c), almost twice the typical decrease that would follow primary productivity, and a 12.0 μM decrease in silicate during 2019 (Figure 9d).

3.3. Higher Trophic Impacts

We briefly explored other biological data to understand potential relationships with higher trophic levels during the summer of 2019 at OSP. We investigated biomass of *Euphausia pacifica* from Line P's station P26 zooplankton tows (Figure 10). *E. pacifica,* or 'krill', are the most abundant zooplankton species to the region (Mackas, 1992) and are prey for higher trophic levels, such as baleen whales. Due to the sparsity of cruise samples taken at P26, there is insufficient data to understand if the primary productivity and enhanced stratification that occurred in the summer of 2019 had an impact on *E. pacifica* biomass. However, it is possible that the data collected by Line P cruises does not fully capture the mobility of *E. pacifica*, as the anomalous conditions observed in 2019 were likely more widespread rather than localized solely to OSP. Therefore, we assessed *E. pacifica* biomass on a wider swath (Figure S3 in Supporting Information S1) which did show some similarities to the chlorophyll concentration.

The increased productivity that occurred in the 2019 summer may have had an impact on higher trophic levels. Blue whales (*Balaenoptera musculus*) have been known to feed as far offshore as OSP (Calambokidis et al., 2009) and have been observed at OSP most often within Aug-Dec (Stafford et al., 1999). While the Noise Reference Station's passive acoustic data set is limited in length (Figure 11), in September 2019, there were 38% more blue whale calls recorded compared to September 2018, suggesting that more blue whales appeared earlier in the foraging season (Aug to Dec) (Stafford et al., 1999, 2007). Across the entire foraging season, more blue whales were present in Aug-Dec 2019 compared to Aug-Dec 2018 (49,879 vs. 45,754 calls) (Figure 11).

4. Summary

In general, the oceanographic environment at Ocean Station Papa (OSP) is complex. Interannual and decadal variations in the atmospheric jet stream and Pacific storm track can lead to a wide range of variability in the northeast (NE) Pacific subarctic gyre and physical environment. Influences of remote processes, such as iron fertilization from wildfires and volcanoes, can impact the physical, biogeochemical, and ecosystem dynamics at

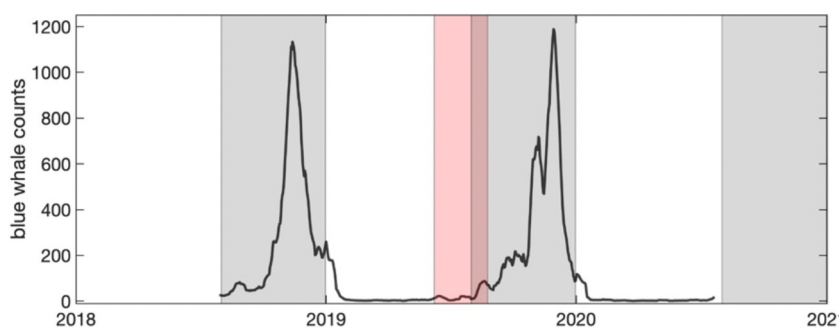

Figure 11. Blue whale B-type calls for July 2018-July 2020 observed from the Noise Reference Station at OSP. Data are shown as a 15-day running average. The red transparent region represents the 2019 MHW period. Gray shaded regions represent prospective foraging seasons (Aug-Dec) of blue whales.

OSP. Our results demonstrate the complexity of understanding the response of the NE Pacific environment to marine heatwaves (MHW) utilizing OSP as a unique laboratory for investigating the cascade of offshore impacts. Although OSP is a point location, many of our observations and conclusions support previous area averaged studies of the 2013–2015 and 2019 MHWs (Figure 2) (Amaya et al., 2020; Bond et al., 2015; Mogen et al., 2022; Scannell et al., 2020) while providing insight into the biogeochemical impacts of the 2019 MHW. Our study is highly localized, thus the local biological responses at OSP may not be fully representative of other MHW biological responses around the globe (e.g., Zhan et al., 2023). OSP provides a unique opportunity to explore the linkages between the physical manifestation of MHWs in the NE Pacific and impacts on biogeochemistry and the ecosystem.

4.1. Connecting the Two Most Recent MHWs in the Northeastern Pacific

Subsurface observations (Figures 3 and 4) at OSP provide critical insights into the potential connection between the two recent MHW events along with interactions with the local ecosystems. The water column was stably stratified due to warm and fresh subsurface conditions prior to and during the 2019 MHW. The temperatures at OSP during the peak SST anomalies in summer of 2019 were anomalous throughout the water column, unlike the 2013–2015 MHW where the subsurface temperature anomalies did not reach beyond 150 m (Figure 3a). Subsurface temperature anomalies associated with the 2013–2015 MHW appeared to have been subducted into deeper waters that could have connected the 2013–2015 and 2019 MHWs as previously noted by Scannell et al. (2020). We also found a strong salinity-stratified barrier layer (Figure 3a) that persisted between the two MHWs and helped to sustain the deep warm anomalies in-between the events. Following the barrier layer, the upper ocean remained anomalously fresh (Figure 4a). Scannell et al. (2020) pointed out that there was an increase in precipitation across the Gulf of Alaska that made the upper ocean more buoyant in 2018. Since OSP did not directly measure strong precipitation signals (S1), the fresh anomalies were likely a result of freshwater advection.

4.2. Impacts of Stratification on Biogeochemistry

There was a large decrease in surface DIC and pCO_2 along with higher than normal surface pH during the 2019 MHW (Figure 8). The decrease in DIC could have been a result of increased stratification and coincident changes in circulation that were observed in 2019 at OSP, similar to the conditions observed during the 2013–2015 MHW as suggested by Mogen et al. (2022) and Franco et al. (2021); however, the increase in productivity observed in the 2019 summer may have also contributed to this decrease in DIC.

4.3. Pre-Conditioning of the Upper Ocean for Warm Temperatures Through a Shallow Mixed Layer and Air-Sea Fluxes

The local heat flux anomalies for both the 2013–2015 and 2019 MHWs at OSP were relatively small compared to the area-average values documented by Schmeisser et al. (2019), Amaya et al. (2020), and Bond et al. (2015). OSP is located at the northern edge of the aforementioned studies (as seen in Figures 2a and 2b). However, there were anomalous shortwave radiative fluxes prior to the 2019 MHW and stratification anomalies at OSP. Since the mixed layer is very thin during the summer in the Gulf of Alaska, the perturbations of the mixed layer have a direct influence on the sea surface temperature tendency, and the mixed layer depth perturbation likely dominates the SST variability (Amaya et al., 2020). Thus, the shallow mixed layer and anomalously high shortwave heat flux into the ocean could explain the extreme intensification of the 2019 SST anomalies at OSP.

4.4. Impacts of Available Chemical Nutrients and Stratification on Productivity

Although there are generally only three cruise samples at Line P Station 26 per year, the cruises in 2019 occurred directly before and after the MHW peak allowing us to analyze impacts biological productivity surrounding the MHW through in situ observations. Coincident with the increased stratification leading up to the MHW of 2019, there was an increase in primary productivity in June at OSP (relative to prior summer samples taken at Line P Station P26 within 2013–2020). Line P collected samples at P26 at the beginning (Jun 10) and at the end (Aug 24) of the MHW of 2019 (Jun 8–Aug 25). In June, there was an increase in chlorophyll and negative AOU, followed by a decrease of silicate and depletion of nitrate in August (Figure 9).

It is likely that there were other processes at play that drove the productivity other than the MHW itself. There was also the possibility of iron enrichment, a limiting factor for larger phytoplankton (Wyatt et al., 2022), which could also have contributed to a large phytoplankton bloom and coincident decreases in nitrate and silicate between the June and August cruises in 2019 (Figure 9). The surface pCO_2 decline and surface pH increase during 2019 at OSP are consistent with pCO_2 and pH observations made during a phytoplankton bloom in the Gulf of Alaska that resulted from volcanic ash iron input in August 2008 (Hamme et al., 2010). Similar to Hamme et al. (2010), there was also evidence of iron deposited from atmospheric dust into surface waters near OSP during the peak of the 2019 MHW (Long et al., 2021; Figure S2 in Supporting Information S1). Thus, the MHW's shallow mixed layer might have worked in concert with the iron-enriched dust deposition to support an increase in productivity. The observed biological productivity that coincided with the 2019 MHW is likely the outcome of a very intricate and complex series of events. To thoroughly understand the biological influences of MHWs worldwide, additional comprehensive biogeochemistry and biological time series, along with further analyses, are necessary.

Other recent MHWs have been shown to have negative effects on higher trophic levels closer to shore (Barlow et al., 2023; Cavole et al., 2016). At OSP in 2019, an offshore site, it appears that there might have been a slightly positive effect on higher trophic levels. There was indication that blue whales came earlier in their foraging season and in greater numbers than in the previous year (Figure 11); however, there is not a clear connection between productivity and krill (Figure 10) due to data limitations. The krill data is collected three times a year at Line P's P26 Station, whereas the acoustic data is continuously recorded from all directions surrounding OSP. The different temporal and spatial data collection techniques cause further challenges to connecting blue whale behavior to the krill abundance.

5. Conclusion

The long-term multi-disciplinary time series at OSP allows insight into the evolution and impacts of MHWs. Due to the relatively short records, gaps, and limited spatial extent in the observational data sets, this analysis should be considered as a case study of the conditions associated with the 2019 NE Pacific MHW at OSP, rather than generalized relationships expected with MHWs at specific locations. The enhanced stratification associated with the 2019 MHW increased the impact of the surface heat flux on the upper ocean temperature leading to extreme warming. The enhanced stratification also impacted productivity by providing a well-lit and nutrient-rich upper ocean for primary producers that led to a bloom in productivity coinciding with the extreme temperatures. The relationship between the 2019 MHW, increased productivity and the early arrival of blue whales along with increased stratification and de-acidification at OSP should be considered speculative, rather than definitive. In addition, the increase in primary production may not have been a direct result of the MHW. It could also be explained by coincident iron fertilization associated with a volcanic eruption that occurred at the same time as the MHW (e.g., Long et al., 2021).

This analysis demonstrates the potential cascade of impacts that occurred during the 2019 MHW. Our holistic approach demonstrates the complexity of the system's response to an extreme event and suggests that MHWs can cause a cascade of impacts owing to changes in both the physical and biogeochemical environment. We also demonstrate the importance of long multi-disciplinary time series for the study of the evolution of both the physical and biogeochemical environment of MHWs and for understanding the connections to higher trophic levels. This suggests the benefits of interdisciplinary time series such as OSP for understanding MHW impacts and interdisciplinary connections.

Data Availability Statement

Surface meteorological variables (winds, air temperature, humidity, barometric pressure, downwelling solar and longwave radiation, rain), bulk air-sea momentum, heat, and moisture fluxes, seawater temperature (surface to 300 m), salinity (surface to 300 m), surface and 35 m currents at the NOAA surface mooring, provided by the OCS Group, are available from the OCS website at https://www.pmel.noaa.gov/ocs/data/disdel/ (Pacific Marine Environmental Laboratory, 2023). Surface air pCO2, seawater pCO2 and pH at the NOAA surface mooring, provided by the PMEL Carbon Group data are available from NCEI, https://doi.org/10.3334/cdiac/otg.tsm_papa_145w_50n (Sutton et al., 2012). Subsurface temperature and salinity mooring data and cruise data (chlorophyll, oxygen, nitrate plus nitrite, and sulfite) at OOI's Global Station Papa Array are available at the NSF OOI Data

Explorer (https://ooinet.oceanobservatories.org/), based upon work supported by the OOI, a major facility fully funded by the NSF under Cooperative Agreement No. 1743430, and the Woods Hole Oceanographic Institution OOI Program Office (NSF Ocean Observatories Initiative, 2022). Significant wave height data from the APL-UW Waverider Mooring (Thomson et al., 2013) were furnished by the Coastal Data Information Program, Integrative Oceanography Division, operated by the Scripps Institution of Oceanography, under the sponsorship of the U.S. Army Corps of Engineers and the California Department of Parks and Recreation (Coastal Data Information Program, 2022, https://doi.org/10.18437/C7WC72). Passive acoustic data from the Noise Reference Station are available from NCEI, https://doi.org/10.7289/V5M32T0D (NOAA OAR Pacific Marine Environmental Laboratory, National Marine Fisheries Service, NOS Office of National Marine Sanctuaries, and DOI NPS Natural Resource Stewardship and Science Directorate, 2014). *Euphausia pacifica* dry weight biomass, chlorophyll concentrations, nitrate plus nitrite, sulfite, and oxygen observations at Station P26 were collected and made freely available by the Institute of Ocean Sciences (Canadian Department of Fisheries and Oceans) as part of the Line P monitoring surveys of the Gulf of Alaska (DFO, 2023). Data can be accessed through their Water Properties Group website at: https://waterproperties.ca/linep. Historical nitrate, nitrite, and silicate shipboard data along Line P are available through the PACIFICA database (Suzuki et al., 2013, https://doi.org/10.25921/n9nn-8324). Sea surface temperature anomaly maps were created using the NOAA OI SST V2 High Resolution Data set data provided by the NOAA PSL, Boulder, Colorado, USA, from their website at https://psl.noaa.gov/data/gridded/data.noaa.oisst.v2.highres.html (Huang et al., 2020). Argo float subsurface temperature and salinity data were collected and made freely available by the International Argo Program and the national programs that contribute to it and are available at https://argo.ucsd.edu/data/data-from-gdacs/ and https://www.ocean-ops.org (Argo, 2000). The Argo Program is part of the Global Ocean Observing System.

Acknowledgments

This project would not have been possible without the help and support from the Ocean Climate Stations Group, Acoustics Group, and Carbon Group. Observations were supported by the NOAA NMFS Office of Science and Technology (OST), NOAA Global Ocean Monitoring and Observing (GOMO), DFO Line P Program, NOAA Ocean Acidification Program, and the National Science Foundation. This material is based upon work supported by the Ocean Observatories Initiative (OOI), a major facility fully funded by the National Science Foundation under Cooperative Agreement No. 1743430, and the Woods Hole Oceanographic Institution OOI Program Office. Funding for CK was provided by the NOAA Ernest F. Hollings Undergraduate Scholarship Program, University of Washington, and a fellowship from the American Meteorological Society. This material is also based on the work supported by the National Science Foundation under Grant 2022874. This publication is partially funded by the Cooperative Institute for Climate, Ocean, and Ecosystem Studies (CIOCES) under NOAA Cooperative Agreement NA20OAR4320271, Contribution No. 2023–1269. This is PMEL contribution number 5344.

References

Alford, M. H., Cronin, M. F., & Klymak, J. M. (2012). Annual cycle and depth penetration of wind-generated near-inertial internal waves at Ocean Station Papa in the northeast Pacific. *Journal of Physical Oceanography*, *42*(6), 889–909. https://doi.org/10.1175/jpo-d-11-092.1

Amaya, D. J., Miller, A. J., Xie, S.-P., & Kosaka, Y. (2020). Physical drivers of the summer 2019 North Pacific marine heatwave. *Nature Communications*, *11*(1), 1903. https://doi.org/10.1038/s41467-020-15820-w

Argo. (2000). Argo float data and metadata from global data assembly centre (Argo GDAC) [Dataset]. *SEANOE*. https://doi.org/10.17882/42182. Accessed June 2022

Barlow, D. R., Klinck, H., Ponirakis, D., Branch, T. A., & Torres, L. G. (2023). Environmental conditions and marine heatwaves influence blue whale foraging and reproductive effort. *Ecology and Evolution*, *13*(2). https://doi.org/10.1002/ece3.9770

Belka, D. J., Schwendeman, M., Thomson, J., & Cronin, M. F. (2014). *Historical wave and wind observations at Ocean Station P. Technical report no. 1407*. Washington University Seattle Applied Physics Lab.

Benson, B. B., & Krause, Jr., D. (1984). The concentration and isotopic fractionation of oxygen dissolved in freshwater and seawater in equilibrium with the atmosphere. *Limnology & Oceanography*, *29*(3), 620–632. https://doi.org/10.4319/lo.1984.29.3.0620

Bond, N. A., Cronin, M. F., Freeland, H., & Mantua, N. (2015). Causes and impacts of the 2014 warm anomaly in the NE Pacific. *Geophysical Research Letters*, *42*(9), 3414–3420. https://doi.org/10.1002/2015gl063306

Calambokidis, J., Barlow, J., Ford, J. K. B., Chandler, T. E., & Douglas, A. B. (2009). Insights into the population structure of blue whales in the Eastern North Pacific from recent sightings and photographic identification. *Marine Mammal Science*, *25*(4), 816–832. https://doi.org/10.1111/j.1748-7692.2009.00298.x

Capotondi, A., Newman, M., Xu, T., & Di Lorenzo, E. (2022). An optimal precursor of northeast Pacific marine heatwaves and central pacific El Niño events. *Geophysical Research Letters*, *49*(5). https://doi.org/10.1029/2021gl097350

Cavole, L. M., Demko, A. M., Diner, R. E., Giddings, A., Koester, I., Pagniello, C. M. L. S., et al. (2016). Biological impacts of the 2013–2015 warm-water anomaly in the northeast Pacific: Winners, Losers, and the future. *Oceanography*, *29*(2), 273–285. https://doi.org/10.5670/oceanog.2016.32

Cheung, W. W. L., & Frölicher, T. L. (2020). Marine heatwaves exacerbate climate change impacts for fisheries in the northeast Pacific. *Scientific Reports*, *10*(1), 1–10. https://doi.org/10.1038/s41598-020-63650-z

Coastal Data Information Program. (2022). Coastal data information program integrative Oceanography division, operated by the Scripps institution of Oceanography, under the sponsorship of the U.S [Dataset]. *Army Corps of Engineers and the California Department of Parks and Recreation*. https://doi.org/10.18437/C7WC72. Accessed June 2022

Cronin, M. F., Anderson, N. D., Zhang, D., Berk, P., Wills, S. M., Serra, Y., et al. (2023). PMEL Ocean Climate Stations as reference time series and research aggregate devices. *Oceanography*, *36*(2–3), 4653. https://doi.org/10.5670/oceanog.2023.224

Cronin, M. F., Pelland, N. A., Emerson, S. R., & Crawford, W. R. (2015). Estimating diffusivity from the mixed layer heat and salt balances in the North Pacific. *Journal of Geophysical Research: Oceans*, *120*(11), 7346–7362. https://doi.org/10.1002/2015jc011010

Cummins, P. F., & Freeland, H. J. (2007). Variability of the North Pacific current and its bifurcation. *Progress in Oceanography*, *75*(2), 253–265. https://doi.org/10.1016/j.pocean.2007.08.006

de Boyer Montégut, C., Madec, G., Fischer, A. S., Lazar, A., & Iudicone, D. (2004). Mixed layer depth over the global ocean: An examination of profile data and a profile-based climatology. *Journal of Geophysical Research*, *109*(C12). https://doi.org/10.1029/2004jc002378

Dickson, A. G. (1990). Standard potential of the reaction: AgCl(s) + 12H2(g) = Ag(s) + HCl(aq), and the standard acidity constant of the ion HSO4− in synthetic sea water from 273.15 to 318.15 K. *The Journal of Chemical Thermodynamics*, *22*(2), 113–127. https://doi.org/10.1016/0021-9614(90)90074-z

Dickson, A. G., & Millero, F. J. (1987). A comparison of the equilibrium constants for the dissociation of carbonic acid in seawater media. *Deep-Sea Research, Part A: Oceanographic Research Papers*, *34*(10), 1733–1743. https://doi.org/10.1016/0198-0149(87)90021-5

Di Lorenzo, E., & Mantua, N. (2016). Multi-year persistence of the 2014/15 North Pacific marine heatwave. *Nature Climate Change*, *6*(11), 1042–1047. https://doi.org/10.1038/nclimate3082

Dziak, R. P., Haxel, J. H., LauHeimlich, T. K. S., Caplan-Auerbach, J., Mellinger, D. K., Matsumoto, H., & Mate, B. (2017). A pulsed-air model of blue whale B call vocalizations. *Scientific Reports*, *7*(9122), 9122. https://doi.org/10.1038/s41598-017-09423-7

Dziak, R. P., Lee, W. S., Haxel, J. H., Matsumoto, H., Tepp, G., Lau, T. K., et al. (2019). Hydroacoustic, meteorologic and seismic observations of the 2016 nansen ice shelf calving event and Iceberg formation. *Frontiers in Earth Science*, *7*. https://doi.org/10.3389/feart.2019.00183

Fairall, C. W., Bradley, E. F., Hare, J. E., Grachev, A. A., & Edson, J. B. (2003). Bulk parameterization of air–sea fluxes: Updates and verification for the COARE algorithm. *Journal of Climate*, *16*(4), 571–591. https://doi.org/10.1175/1520-0442(2003)016<0571:BPOASF>2.0.CO;2

Fisheries and Oceans Canada (DFO). (2023). Line P program cruise data [Dataset]. *Institute of Ocean Sciences*. Retrieved from https://waterproperties.ca/linep. Accessed June 2022

Franco, A. C., Ianson, D., Ross, T., Hamme, R. C., Monahan, A. H., Christian, J. R., et al. (2021). Anthropogenic and climatic contributions to observed carbon system trends in the northeast Pacific. *Global Biogeochemical Cycles*, *35*(7). https://doi.org/10.1029/2020gb006829

Freeland, H. (2007). A short history of Ocean station Papa and line P. *Progress in Oceanography*, *75*(2), 120–125. https://doi.org/10.1016/j.pocean.2007.08.005

Garcia, H. E., & Gordon, L. I. (1992). Oxygen solubility in seawater: Better fitting equations. *Limnology & Oceanography*, *37*(6), 1307–1312. https://doi.org/10.4319/lo.1992.37.6.1307

Garcia, H. E., & Gordon, L. I. (1993). Erratum: Oxygen solubility in seawater: Better fitting equations. *Limnology & Oceanography*, *38*(3), 656. https://doi.org/10.4319/lo.1993.38.3.0643

Hamme, R. C., Webley, P. W., Crawford, W. R., Whitney, F. A., DeGrandpre, M. D., Emerson, S. R., et al. (2010). Volcanic ash fuels anomalous plankton bloom in subarctic northeast Pacific. *Geophysical Research Letters*, *37*(19). https://doi.org/10.1029/2010gl044629

Harrison, P. J. (2002). Station Papa time series: Insights into ecosystem dynamics. *Journal of Oceanography*, *58*(2), 259–264. https://doi.org/10.1023/a:1015857624562

Harrison, P. J., Boyda, P. W., Varela, D. E., Takeda, S., Shiomoto, A., & Odate, T. (1999). Comparison of factors controlling phytoplankton productivity in the NE and NW subarctic Pacific gyres. *Progress in Oceanography*, *43*(2–4), 205–234. https://doi.org/10.1016/s0079-6611(99)00015-4

Harrison, P. J., Whitney, F. A., Tsuda, A., Saito, H., & Tadokoro, K. (2004). Nutrient and plankton dynamics in the NE and NW gyres of the subarctic pacific ocean. *Journal of Oceanography*, *60*(1), 93–117. https://doi.org/10.1023/b:joce.0000038321.57391.2a

Hartmann, D. L. (2015). Pacific sea surface temperature and the winter of 2014. *Geophysical Research Letters*, *42*(6), 1894–1902. https://doi.org/10.1002/2015gl063083

Hayashida, H., Matear, R. J., & Strutton, P. G. (2020). Background nutrient concentration determines phytoplankton bloom response to marine heatwaves. *Global Change Biology*, *26*(9), 4800–4811. https://doi.org/10.1111/gcb.15255

Hobday, A. J., Alexander, L. V., Perkins, S. E., Smale, D. A., Straub, S. C., Oliver, E. C. J., et al. (2016). A hierarchical approach to defining marine heatwaves. *Progress in Oceanography*, *141*(0079–6611), 227–238. https://doi.org/10.1016/j.pocean.2015.12.014

Holbrook, N. J., Scannell, H. A., Sen Gupta, A., Benthuysen, J. A., Feng, M., Oliver, E. C. J., et al. (2019). A global assessment of marine heatwaves and their drivers. *Nature Communications*, *10*(1), 2624. https://doi.org/10.1038/s41467-019-10206-z

Holbrook, N. J., Sen Gupta, A., Oliver, E. C. J., Hobday, A. J., Benthuysen, J. A., Scannell, H. A., et al. (2020). Keeping pace with marine heatwaves. *Nature Reviews Earth and Environment*, *1*(9), 482–493. https://doi.org/10.1038/s43017-020-0068-4

Huang, B., Liu, C., Banzon, V., Freeman, E., Graham, G., Hankins, B., et al. (2020). Improvements of the daily Optimum interpolation Sea Surface temperature (DOISST) version 2.1 [Dataset]. *Journal of Climate*, *34*(8), 2923–2939. https://doi.org/10.1175/JCLI-D-20-0166.1. Accessed June 2022

Katsura, S., Oka, E., & Sato, K. (2015). Formation mechanism of barrier layer in the subtropical pacific. *Journal of Physical Oceanography*, *45*(11), 2790–2805. https://doi.org/10.1175/jpo-d-15-0028.1

Lewis, E., & Wallace, D. W. R. (1998). *Program developed for CO2 system calculations, ORNL/CDIAC-105*. Oak Ridge National Lab. https://doi.org/10.15485/1464255

Long, J. S., Fassbender, A. J., & Estapa, M. L. (2021). Depth resolved net primary production in the northeast Pacific ocean: A comparison of satellite and profiling float estimates in the context of two marine heatwaves. *Geophysical Research Letters*, *48*(19). https://doi.org/10.1029/2021gl093462

Lukas, R., & Lindstrom, E. (1991). The mixed layer of the western equatorial Pacific Ocean. *Journal of Geophysical Research*, *96*(S01), 3343–3357. https://doi.org/10.1029/90jc01951

Mackas, D. L. (1992). Seasonal cycle of zooplankton off Southwestern British Columbia: 1979–89. *Canadian Journal of Fisheries and Aquatic Sciences*, *49*(5), 903–921. https://doi.org/10.1139/f92-101

Mackas, D. L. (1995). Interannual variability of the zooplankton community off southern Vancouver Island. *Climate change and northern fish populations*, *121*, 603–615.

McDougall, T. J., & Barker, P. M. (2011). Getting started with TEOS-10 and the Gibbs seawater (GSW) oceanographic Toolbox, 28, SCOR/IAPSO WG127. ISBN 978-0-646-55621-5.

Mehrbach, C., Culberson, C. H., Hawley, J. E., & Pytkowicx, R. M. (1973). Measurement of the apparent dissociation constants of carbonic acid in seawater at atmospheric pressure. *Limnology & Oceanography*, *18*(6), 897–907. https://doi.org/10.4319/lo.1973.18.6.0897

Mellinger, D. K. (2001). *Ishmael 1.0 user's guide*. NOAA Technical Memorandum OAR PMEL-120. Available from NOAA/PMEL/OERD, 2115 SE OSU Drive, Newport, Oregon http://www.pmel.noaa.gov/pubs/PDF/mell2434/mell2434.pdf

Mellinger, D. K. (2004). A comparison of methods for detecting right whale calls. *Canadian Acoustics*, *32*(55–65).

Mellinger, D. K., & Clark, C. W. (2000). Recognizing transient low-frequency whale sounds by spectrogram correlation. *Journal of the Acoustical Society of America*, *107*(6), 3518–3529. https://doi.org/10.1121/1.429434

Mogen, S. C., Lovenduski, N. S., Dallmann, A. R., Gregor, L., Sutton, A. J., Bograd, S. J., et al. (2022). Ocean biogeochemical signatures of the North Pacific Blob. *Geophysical Research Letters*, *49*(9). https://doi.org/10.1029/2021gl096938

NOAA OAR Pacific Marine Environmental LaboratoryNational Marine Fisheries Service, NOS Office of National Marine Sanctuaries, and DOI NPS Natural Resource Stewardship and Science Directorate. (2014). *NOAA Ocean noise reference station network raw passive acoustic data*. NOAA National Centers for Environmental Information. https://doi.org/10.7289/V5M32T0D. Accessed June 2021.

Noh, K. M., Lim, H.-G., & Kug, J.-S. (2022). Global chlorophyll responses to marine heatwaves in satellite ocean color. *Environmental Research Letters*, *17*(6), 064034. https://doi.org/10.1088/1748-9326/ac70ec

NSF Ocean Observatories Initiative. (2022). Subsurface CTD (GP03FLMB-RIM01-02 CTDMOH070) data from flanking subsurface moorings A and B and cruise (MV1309, MV1404, RB1605, SKQ201920S, SR1710, SR1811, TN323) data at global station Papa from 2013-01-01 to 2020-12-31. Retrieved from https://ooinet.oceanobservatories.org/. Accessed June 2022.

Pacific Marine Environmental Laboratory. (2023). Ocean station Papa (50.1°N, 144.9°W) mooring data [Dataset]. *NOAA OAR-PMEL Ocean Climate Stations*. Retrieved from https://www.pmel.noaa.gov/ocs/data/disdel/. Accessed January 2023

Scannell, H. A., Johnson, G. C., Thompson, L., Lyman, J. M., & Riser, S. C. (2020). Subsurface evolution and persistence of marine heatwaves in the northeast Pacific. *Geophysical Research Letters*, *47*(23). https://doi.org/10.1029/2020gl090548

Schmeisser, L., Bond, N. A., Siedlecki, S. A., & Ackerman, T. P. (2019). The role of clouds and surface heat fluxes in the maintenance of the 2013–2016 northeast Pacific marine heatwave. *Journal of Geophysical Research: Atmospheres*, *124*(20), 10772–10783. https://doi.org/10.1029/2019jd030780

Smale, D. A., Wernberg, T., Oliver, E. C. J., Thomsen, M., Harvey, B. P., Straub, S. C., et al. (2019). Marine heatwaves threaten global biodiversity and the provision of ecosystem services. *Nature Climate Change*, *9*(4), 306–312. https://doi.org/10.1038/s41558-019-0412-1

Stafford, K., Citta, J., Moore, S., Daher, M., & George, J. (2009). Environmental correlates of blue and fin whale call detections in the North Pacific Ocean from 1997 to 2002. *Marine Ecology Progress Series*, *395*, 37–53. https://doi.org/10.3354/meps08362

Stafford, K. M., Mellinger, D. K., Moore, S. E., & Fox, C. G. (2007). Seasonal variability and detection range modeling of baleen whale calls in the Gulf of Alaska, 1999–2002. *Journal of the Acoustical Society of America*, *122*(6), 3378–3390. https://doi.org/10.1121/1.2799905

Stafford, K. M., Nieukirk, S. L., & Fox, C. G. (1999). AN acoustic link between blue whales in the eastern tropical pacific and the northeast Pacific1. *Marine Mammal Science*, *15*(4), 1258–1268. https://doi.org/10.1111/j.1748-7692.1999.tb00889.x

Sutton, A. J., Sabine, C. L., Dietrich, C., Maenner-Jones, S., Musielewicz, S., Bott, R., & Osborne, J. (2012). High-resolution ocean and atmosphere pCO2 time-series measurements from mooring Papa_145W_50N in the North Pacific Ocean (NCEI Accession 0100074) [Dataset]. *NOAA National Centers for Environmental Information*. Jan 2013 - Dec 2020. https://doi.org/10.3334/cdiac/otg.tsm_papa_145w_50n. Accessed October 2023

Sutton, A. J., Sabine, C. L., Feely, R. A., Cai, W.-J., Cronin, M. F., McPhaden, M. J., et al. (2016). Using present-day observations to detect when anthropogenic change forces surface ocean carbonate chemistry outside preindustrial bounds. *Biogeosciences*, *13*(17), 5065–5083. https://doi.org/10.5194/bg-13-5065-2016

Sutton, A. J., Sabine, C. L., Maenner-Jones, S., Lawrence-Slavas, N., Meinig, C., Feely, R. A., et al. (2014). A high-frequency atmospheric and seawater pCO_2 data set from 14 open-ocean sites using a moored autonomous system. *Earth System Science Data*, *6*(2), 353–366. https://doi.org/10.5194/essd-6-353-2014

Suzuki, T., Ishii, M., Aoyama, M., Christian, J., Enyo, K., Kawano, T., et al. (2013). The pacific ocean interior carbon (PACIFICA) database (NCEI accession 0110865) [Dataset]. *NOAA National Centers for Environmental Information*. https://doi.org/10.25921/n9nn-8324. Accessed June 2022

Thomson, J., D'Asaro, E. A., Cronin, M. F., Rogers, W. E., Harcourt, R. R., & Shcherbina, A. (2013). Waves and the equilibrium range at Ocean weather station P. *Journal of Geophysical Research: Oceans*, *118*(11), 5951–5962. https://doi.org/10.1002/2013jc008837

van Heuven, S., Rae, J. W. B., Wallace, D. W. R., Lewis, E., & Pierrot, D. (2011). MATLAB program developed for CO2 system calculations [Software]. *Carbon Dioxide Information Analysis Center, ORNL/CDIAC-105b*. https://doi.org/10.3334/cdiac/otg.co2sys_matlab_v1.1

Whitney, F., Wong, C., & Boyd, P. (1998). Interannual variability in nitrate supply to surface waters of the Northeast Pacific Ocean. *Marine Ecology Progress Series*, *170*, 15–23. https://doi.org/10.3354/meps170015

Whitney, F. A., & Freeland, H. J. (1999). Variability in upper-ocean water properties in the NE Pacific Ocean. *Deep Sea Research Part II: Topical Studies in Oceanography*, *46*(11–12), 2351–2370. https://doi.org/10.1016/s0967-0645(99)00067-3

Wong, C. S., Whitney, F. A., Matear, R. J., & Iseki, K. (1998). Enhancement of new production in the northeast subarctic Pacific Ocean during negative North Pacific index events. *Limnology & Oceanography*, *43*(7), 1418–1426. https://doi.org/10.4319/lo.1998.43.7.1418

Wyatt, A. M., Resplandy, L., & Marchetti, A. (2022). Ecosystem impacts of marine heat waves in the northeast Pacific. *Biogeosciences*, *19*(24), 5689–5705. https://doi.org/10.5194/bg-19-5689-2022

Zhan, W., Zhang, Y., He, Q., & Zhan, H. (2023). Shifting responses of phytoplankton to atmospheric and oceanic forcing in a prolonged marine heatwave. *Limnology & Oceanography*, *68*(8), 1821–1834. https://doi.org/10.1002/lno.12388

Zhang, Y., Du, Y., Feng, M., & Hobday, A. J. (2023). Vertical structures of marine heatwaves. *Nature Communications*, *14*(1), 6483. https://doi.org/10.1038/s41467-023-42219-0